# The impact of eastern Pacific warming on future

# North Atlantic tropical cyclogenesis

Kristopher B. Karnauskas<sup>1,2,\*</sup>, Ulla K. Heede<sup>1</sup>, Lei Zhang<sup>3</sup> 1. Cooperative Institute for Research in Environmental Sciences, University of Colorado, Boulder, CO USA 2. Department of Atmospheric and Oceanic Sciences, University of Colorado, Boulder, CO USA 3. State Key Laboratory of Tropical Oceanography, South China Sea Institute of Oceanology, Chinese Academy of Sciences, Guangzhou, China Corresponding author: kristopher.karnauskas@colorado.edu Revised manuscript submitted to Geophysical Research Letters August 21, 2023

#### Abstract

Tropical cyclogenesis in the Atlantic is influenced by environmental parameters including vertical wind shear, which is sensitive to forcing from the tropical Pacific. Reliable projections of the response of such parameters to radiative forcing are key to understanding the future of hurricanes and coastal risk. One of the least certain aspects of future climate is the warming of the eastern tropical Pacific Ocean. Using climate model experiments isolating the warming of the eastern Pacific and controlling for other factors including El Niño-Southern Oscillation (ENSO), changes in Atlantic tropical cyclogenesis potential by the end of this century are ~20% lower with enhanced eastern Pacific warming. The ENSO signal in Atlantic tropical cyclogenesis potential amplifies with global warming, and that amplification is larger with enhanced eastern Pacific warming. The largest changes and dependencies on eastern Pacific warming are found in the south-central main development region, attributable to changes in zonal overturning.

## **Key Points**

- Enhanced surface warming in the eastern equatorial Pacific Ocean impacts the response of

  Atlantic hurricanes to global warming.
- Genesis potential decreases in the south-central part of the main development region, but only with enhanced eastern Pacific warming.
  - The El Niño/La Niña signal in Atlantic genesis potential amplifies with global warming—more so with enhanced eastern Pacific warming.

#### Plain Language Summary

Today, there are about 15 tropical storms per year in the Atlantic. That number varies considerably from year to year, with El Niño being one major factor. When the eastern Pacific Ocean warms temporarily, Atlantic hurricanes tend to be suppressed (and vice versa for La Niña). As the climate warms due to greenhouse gas emissions, hurricanes are expected to change. Such changes could include the average number of tropical storms per year, where they tend to form, how strong they become, how far and fast they travel, how much rain they produce, and how El Niño affects them. This study investigates how the formation regions of Atlantic hurricanes may change in the future, particularly as a function of how much the eastern Pacific Ocean warms in the future, which is one of the most uncertain aspects of climate change. We find that the warming of the eastern Pacific strongly influences predictions of future changes in Atlantic hurricanes, including how El Niño affects them. Specifically, a strong eastern Pacific warming causes a change in the winds over the tropical Atlantic, which shifts where hurricanes will tend to form in the future, and increases the effect of El Niño.

#### 1. Introduction

North Atlantic tropical cyclones (TCs) pose significant risk to coastal regions from the Mid-Atlantic to the Caribbean (Peduzzi et al., 2012; Klotzbach et al., 2018). As their genesis and subsequent development are closely related to such large-scale environmental parameters as sea surface temperature (SST; Emanuel, 2005) and vertical wind shear (Gray, 1968), it is no surprise that a great deal of research effort has been dedicated to understanding how TCs may change in the future under climate change (Knutson et al., 2020). Such investigations usually rely on global models that simulate changes in large-scale environmental parameters but are not capable of explicitly resolving TCs (a form of statistical downscaling; Villarini and Vecchi, 2012), regional models that resolve TCs but are subject to changes in environmental parameters prescribed from global models (dynamical downscaling; Knutson et al., 1998), global models that resolve TCs within a changing environment despite the computational expense (Chu et al., 2020; van Westen et al., 2023), or a hybrid approach in which an extremely high resolution TC model is allowed to roam within the output of global models post boe (Emanuel et al., 2008; Zhang et al., 2017; Karnauskas et al., 2021).

Shorter term, natural fluctuations in climate are also known to modulate the level of Atlantic hurricane activity—in particular, the El Niño-Southern Oscillation (ENSO; Lin et al., 2021). Specifically, Atlantic hurricane activity tends to be suppressed during the El Niño phase, and elevated during the La Niña phase, primarily due to the remote influence of eastern tropical Pacific SST anomalies on vertical wind shear over the Atlantic (Goldenberg and Shapiro, 1996; Aiyyer and Thorncroft, 2006; 2011). In fact, the perceived importance of ENSO's influence rivals that of local SST in the Atlantic main development region (MDR). On May 25, 2023, for example, despite above-average Atlantic Ocean temperatures, the National Oceanic and Atmospheric Administration (NOAA) called for a 40% chance of "near-normal" Atlantic hurricane activity due to the ongoing and forecasted development of El Niño conditions (NOAA, 2023).

It is reasonable to hypothesize that future changes in Atlantic hurricane activity will, to an extent, be a function of changes in the eastern tropical Pacific. How the average conditions of climate may change in the future, and how natural modes of variability and their remote influences may change, are separate but intertwined questions. In the case of the tropical Pacific, these questions have considerable uncertainty and are subject to vigorous debate within the climate dynamics community (Lee et al., 2022). For several generations of coupled climate models, the consensus projection has featured an enhanced surface warming of the eastern tropical Pacific Ocean (Knutson and Manabe, 1995; Vecchi and Soden, 2007; Coats and Karnauskas, 2017; Fredriksen et al., 2020; Heede and Fedorov, 2021). One reason for hesitation to simply accept this projection, despite the physical mechanisms being reasonably well articulated and understood, lies in its persistent and profound discrepancy with historical records of SST (Karnauskas et al., 2009; Seager et al., 2022; Heede and Fedorov, 2023a). Moreover, the ability of global climate models to adequately represent the key physical processes in the equatorial ocean and its coupling with the atmosphere have recently been called into question due to persistent model biases in the eastern tropical Pacific (Coats and Karnauskas, 2018; Seager et al., 2019; Karnauskas et al., 2020). Sobel et al. (2023) recently called attention to the consequences of such uncertainties for future TC projections, and motivated the development of projections that represent a broader range of future changes in the tropical Pacific.

79

80

81

82

83

84

85

86

87

88

89

90

91

92

93

94

95

96

97

98

99

100

101

102

For the question of future ENSO changes, the underlying uncertainty resides less in model-observation discrepancy (as we know we are unlikely to have long enough historical records to attribute—or even detect changes in ENSO; Wittenberg, 2009), and more in the spread among similarly-constructed models (Collins et al., 2010). While the majority of Coupled Model Intercomparison Project phase 6 (CMIP6) models project a significant change in ENSO with anthropogenic forcing (Cai et al., 2022), the response varies widely depending on type of experiment, timeframe, and model (Maher et al., 2023; Heede and Fedorov, 2023b), which leaves low confidence

in our current ability to project changes to ENSO. Moreover, even if ENSO variability does not respond to anthropogenic forcing, the teleconnections linking ENSO to remote basins—particularly the North Atlantic, are sensitive to changes in the mean state (Drouard and Cassou, 2019). Therefore, to consider the future changes of impacts that depend upon the tropical Pacific such as Atlantic hurricane activity, one is plagued by both a relatively robust mean-state projection that is at odds with historical records, and by wildly unconstrained changes in variability where coupled modes and mean-state dependent teleconnections are mixed.

In this study, we examine a suite of global model experiments designed to circumvent these issues. Our experiments strictly control for ENSO variability, while embracing both potential future mean state changes (with and without enhanced eastern Pacific warming). Therefore, our analyses expose the range of uncertainty in future Atlantic hurricane activity as a function of this key aspect of climate change projections, without the confounding factor introduced by using multiple models. This set of experiments is used to understand both the future change in average conditions in the North Atlantic of relevance to TCs, and the future change in the impact of ENSO variability on Atlantic hurricane activity. The latter analysis makes the implicit assumption that ENSO itself (including its amplitude, seasonality, and spatial pattern) does not change—leaving the emergent changes in the North Atlantic a function only of the teleconnections as modulated by the changing background state. The model experiments are described in the following section, followed by results, summary and discussion.

#### 2. Methods

- a. Model and experimental design
- The global climate model used in this study is the National Center for Atmospheric Research (NCAR)
- 126 Community Earth System Model, version 2 (CESM2). All of our experiments use prescribed SST and

sea ice boundary conditions, leaving only the atmosphere and land surface as interactive components. The atmospheric component in our experiments is the NCAR Community Atmosphere Model, version 6 (CAM6) with ~1° horizontal resolution and 32 vertical levels. Further details are given by Danabasoglu et al. (2020).

We conduct three experiments, each integrated for 85 years: control, EP, and noEP (Figure 1). The control experiment is integrated with all radiative forcing such as CO<sub>2</sub> concentration held constant at year 2000 levels. The prescribed SST forcing includes the observed seasonal cycle of SST computed over 1982–2001 (Hurrell et al., 2008), and an idealized ENSO cycle (Figures 1d and 1e). The ENSO sequence features a large El Niño, a large La Niña, a smaller El Niño, and a smaller La Niña, with neutral years between each event. The events are phased in and out in a Gaussian fashion, peaking in boreal winter, consistent with observed ENSO behavior. This ENSO sequence spans 10 years, and is repeated 8.5 times to cover the 85-year integration. The spatial pattern of the ENSO events (Figure 1c) is obtained by taking the leading Empirical Orthogonal Function (EOF) of observed, detrended SST anomalies over 1950–2021 from the NOAA Extended Reconstructed SST, version 5 (Huang et al., 2017). The prescribed ENSO cycle is idealized in that the spatial pattern of SST anomalies is constant, and there is neither temporal nor spatial asymmetry between phases.

The EP experiment is similar to control in terms of the SST climatology and idealized ENSO cycle, but with a global SST trend pattern linearly ramped from 2015–2100, obtained from the Representative Concentration Pathway 8.5 (RCP8.5) experiment of the fully coupled version of CESM1 (Figure 1a). The CESM1 forced SST pattern is selected as it exemplifies a typical eastern Pacific warming response and climate sensitivity of current generation climate models. Atmospheric CO<sub>2</sub> increases over time in the EP experiment according to Shared Socioeconomic Pathway 585 (SSP585). The noEP experiment is identical to EP, except that the enhanced warming in the eastern equatorial Pacific Ocean was first removed from the SST trend pattern through an iterative smoothing

technique that ensures that the eastern Pacific warms at the same rate as the tropical mean (Figure 1b). Overall, the homogenization process to construct the noEP forcing involved Pacific SSTs spanning 50°S–20°N. Perturbed initial condition ensembles of five runs apiece were formed for both the EP and noEP experiments. Only a single integration of the control experiment was conducted, but since CO<sub>2</sub> forcing is constant and there is no SST trend, each 10-year segment is considered an independent realization and may be averaged into an 8.5-member quasi-ensemble mean.

b. Diagnostic calculations

In general, the level of TC activity in a given climate is a function of the number of initial disturbances that can develop into TCs (e.g., easterly waves), and the extent to which the large-scale environment supports TC development (Gray, 1968; 1990). In this study, we focus on the latter, and employ the Genesis Potential Index (GPI) to characterize the environment as a function of time and the experimental parameters described above. The GPI, developed by Emanuel and Nolan (2004), has proven to be a useful metric for such applications (Camargo et al., 2007a; Camargo et al., 2007b; Zhang et al., 2017) as it incorporates many of the environmental parameters known to influence TC development including vertical wind shear, lower-tropospheric absolute vorticity, mid-tropospheric relative humidity, and potential intensity—which is a function of SST and tropospheric stability.

Following Emanuel and Nolan (2004) and others, GPI is calculated here as

$$GPI = |10^{5}\eta|^{3/2} \left(\frac{RH}{50}\right)^{3} \left(\frac{V_{pot}}{70}\right)^{3} (1 + 0.1V_{shear})^{-2}$$
 (1)

where  $\eta$  is absolute vorticity at 850 mb, RH is relative humidity at 600 mb,  $V_{pot}$  is potential intensity, and  $V_{shear}$  is the magnitude of vertical wind shear between 250 mb and 850 mb. Following Bister (2002), potential intensity is defined as

$$V_{pot}^2 = \frac{SST}{T_0} \frac{C_k}{C_D} [CAPE^* - CAPE]|_m$$
 (2)

where  $T_0$  is the outflow temperature,  $C_k$  is the exchange coefficient for enthalpy,  $C_D$  is the drag coefficient,  $CAPE^*$  is the convective available potential energy of air lifted from saturation at sea level in reference to the environmental sounding, CAPE is that of boundary layer air, and subscript m indicates evaluation at the radius of maximum winds. In addition to wind shear, an important mechanism for the teleconnection from ENSO to the tropical Atlantic is tropospheric warming by equatorial waves (Tang and Neelin, 2004), which would influence GPI by way of the CAPE term in potential intensity. These parameters are calculated using the monthly outputs of the CESM2 experiments described above, and averages over the official Atlantic hurricane season (June–November) are presented. Before describing the main results, the control experiment is evaluated against the ECMWF Reanalysis, version 5 (ERA5; Hersbach et al., 2020).

#### 3. Results

a. Description and evaluation of the mean state

The control experiment exhibits GPI maxima along the southeastern flank of the canonical MDR, in the southern Caribbean Sea, throughout the Gulf of Mexico, and in the northwestern subtropical Atlantic Ocean (Figure 2f). As anticipated from (1), these regions of relatively high GPI coincide with a confluence of low shear, static instability, high humidity, and warm SST—yet constrained to north of  $\sim$ 5°N, where absolute vorticity is not prohibitively small for the maintenance of gradient wind balance critical to TCs (Figure 2a–e).

With minor exception, the mean fields simulated by CESM2 are similar to those estimated from ERA5 (Figure S1), and it can be seen that maxima in the ERA5 GPI field broadly aligns with observed TC genesis locations over the same time period from in the International Best Track Archive for Climate Stewardship (IBTrACS) dataset (Knapp et al., 2010) (Figure S2). In terms of GPI, the most obvious differences are that CESM2 exhibits lower near the MDR, and higher in the Caribbean,

Gulf of Mexico and northwestern subtropical Atlantic. The former bias appears to be reconcilable through differences in vertical wind shear, while the latter appears related to SST, humidity and stability. Some differences, particularly in thermodynamic parameters, are to be expected given the slight difference in time periods including CO<sub>2</sub> concentrations. Overall, the CESM2-simulated climatological TC environment in the North Atlantic appears suitable for investigating its response to internal and external forcings.

#### b. Changes in the mean state

In response to rising CO<sub>2</sub> and global SST changes, the EP experiment exhibits several GPI changes in key regions of interest (Figure 3). Across most of the MDR from the Caribbean to the central tropical Atlantic, GPI is reduced by up to 24%, accompanied by a very strong increase (over 100%) in the southeastern corner of the MDR extending to the coast of Africa (Figure 3d). Substantial increases in GPI (by 50–100%) also occur throughout the northern Gulf of Mexico and northwestern subtropical Atlantic. Most of the spatial structure of these changes is explained by that of wind shear (Figure 3a), with the exception of the northern Gulf of Mexico and the southward extent of the increase in the northwestern subtropical Atlantic (maximizing in the Sargasso Sea near 32°N). This is confirmed by recalculating the change in GPI where vertical wind shear from the control experiment is used in the GPI calculations for both control and EP (Figure S3). In the northern Gulf of Mexico and northwestern subtropical Atlantic, the increase in GPI is explained by an increase in potential intensity, absolute vorticity and relative humidity. The effect of removing the enhanced eastern Pacific warming is to eliminate the aforementioned GPI reduction in the central MDR, and damp (by ~25%) the increase in GPI near the coast of Africa (Figures 3e and 3f). These intensity of these changes in GPI, including their dependence on the enhanced eastern Pacific warming, are roughly uniform from

the onset of the climatological hurricane season into the peak months, but very weak by November (Figure S4).

The large GPI changes along the southern flank of the MDR can be understood through consideration of vertical wind shear that arises as part of the zonal atmospheric overturning (*i.e.*, the Atlantic Walker cell). In the control experiment, upper-level winds are more westerly than the lower-level winds from about 80–32°W (Figure 4a). East of 32°W, the opposite is the case (meaning the overturning is not Walker-like). The response to rising CO<sub>2</sub> and global SST changes is an increase in the westerly wind at 250 mb—equivalent to a roughly uniform anomaly of 2–4 m/s, and negligible change in the surface easterlies. West of 32°W, this upper-level change serves to increase the initial shear, while east of 32°W, there is a transition to a reduction in shear (by bringing the zonal wind at 250 mb closer to that at 850 mb). The overall change also includes an eastward shift by ~790 km of the location of zero shear. The response in the experiment without enhanced eastern Pacific warming is qualitatively similar, but scaled by about half.

### c. Changes in ENSO's impact

Finally, we examine the influence of global warming, including the specific impact of enhanced eastern Pacific warming, on the ENSO signal in North Atlantic GPI. The control experiment exhibits an ENSO signal consistent with observations, where El Niño reduces Atlantic hurricane activity by lowering GPI along the southern flank of the MDR extending from the coast of Africa into the Caribbean and throughout the Gulf of Mexico and northwestern subtropical Atlantic (Figures 5a and 5e). Under global warming, the ENSO signal is qualitatively similar in most aspects to control, but greatly amplified (Figure 5e) and includes a new anomaly near the coast of Africa where El Niño increases GPI (Figure 5b). With few exceptions, enhanced warming in the eastern Pacific serves to increase these responses (Figure 5d). In the noEP experiment, lack of enhanced eastern Pacific

warming reverses the sign of the ENSO signal in the Gulf of Mexico such that El Niño leads to higher GPI there (Figure 5c). Interestingly, La Niña exhibit higher GPI in the noEP experiment than in control (Fig. 5e), illustrating nonlinearities in the tradeoff between the patterns of background warming versus those of interannual anomalies.

The physical mechanism for the increase in ENSO signal in the south-central MDR region, and the emergence of an opposing signal closer to the African coastline, is analogous to that previously described for the mean state change. El Niño increases the westerly zonal wind at 250 mb, which increases (decreases) shear to the west (east) of the point at which the zonal winds at 250 mb and 850 mb intersect (Figure 4b). This remote response to ENSO is amplified in both EP and noEP experiments relative to control, but more so in the EP experiment (Figures 4c and 4d).

### 4. Summary and Discussion

A suite of global warming experiments that isolate the role of mean state changes in the eastern tropical Pacific reveal the key dependencies of future Atlantic hurricane activity on this highly uncertain aspect of climate change. Overall, we conclude that future Atlantic hurricane activity—both the average statistics and the ENSO signal therein—does depend on whether enhanced warming of the eastern tropical Pacific Ocean is an emergent feature of the climate response to anthropogenic radiative forcing. In some regions, increases in genesis potential are doubled by the presence of enhanced eastern Pacific warming; in the Gulf of Mexico, even the sign of change is sensitive to the level of warming in the eastern Pacific.

In particular, along the southern flank of the MDR, a strong dipole response emerges in the case with enhanced eastern Pacific warming such that genesis potential decreases west of about 32°W and increases east thereof, similar to high-resolution coupled model simulations (Murakami et al., 2012; van Westen et al., 2023). These changes, shown here to be critically dependent on the enhanced

eastern Pacific warming, are associated with a positive (westerly) anomaly in the upper-level zonal winds, which is itself part of a global-scale contraction of the tropical upper-tropospheric easterlies rather than a regional-scale phenomenon (Figure S5). Such a change in a key region of TC development may have considerable implications for coastal risk in the western Atlantic. For example, the eastward shift in the region of maximum GPI may allow westward propagating TCs to spend more time over the relatively warm tropical Atlantic Ocean before approaching land. Given the seasonality of these changes (Figure S4), one may anticipate an earlier onset of the Atlantic hurricane season—but not a lengthening toward winter months. Such development scenarios could be verified through TC-resolving simulations or other downscaling approaches such as those mentioned in the introduction.

Previous studies have revealed several important societal impacts that critically depend on whether the eastern tropical Pacific warms the way generations of models have projected, for example, the drying of the American Southwest (Seager and Vecchi, 2010) and many others (Lee et al., 2022). This study adds one additional, particularly destructive impact to that list, further underscoring the pressing need to resolve the mismatch between historical observations and climate models. Some caution is warranted when interpreting GPI quantitatively in different climates, as the relationships between GPI input parameters and TC genesis may be state dependent. Other regions such as typhoons in the northwestern Pacific are beyond the scope of this study, but may hold considerable sensitivities to the eastern Pacific warming response as well.

#### Acknowledgements

KBK acknowledges funding support from the NSF PREEVENTS program (award 1854956). KBK and UKH acknowledge computing awards from NCAR CISL (awards UCUB0127, UCUB0135, and UCUB0141). UKH acknowledges funding support from the CIRES Visiting Fellows Program. LZ

acknowledges funding support from the State Key Laboratory of Tropical Oceanography (grant 293 294 LTORC2201). 295 296 Data Availability 297 All observational data used in this study are freely and publicly available. 298 ERA5: https://www.ecmwf.int/en/forecasts/dataset/ecmwf-reanalysis-v5 299 NOAA ERSSTv5: https://psl.noaa.gov/data/gridded/data.noaa.ersst.v5.html 300 IBTrACS: https://www.ncei.noaa.gov/products/international-best-track-archive 301 The subset of model output fields required to reproduce the results presented in this study, including 302 genesis potential index (GPI), are deposited in Zenodo: https://doi.org/10.5281/zenodo.8157139.

#### References

- Aiyyer, A. R., and C. Thorncroft, 2006: Climatology of Vertical Wind Shear over the Tropical Atlantic.
- 305 *J. Climate*, 19, 2969–2983, <a href="https://doi.org/10.1175/JCLI3685.1">https://doi.org/10.1175/JCLI3685.1</a>.
- 306 Aiyyer, A., and C. Thorncroft, 2011: Interannual-to-Multidecadal Variability of Vertical Shear and
- 307 Tropical Cyclone Activity. J. Climate, 24, 2949–2962,
- 308 https://doi.org/10.1175/2010JCLI3698.1.
- 309 Bister, M. (2002). Low frequency variability of tropical cyclone potential intensity 1. Interannual to
- 310 interdecadal variability. Journal of Geophysical Research, 107(D24), 4801.
- 311 https://doi.org/10.1029/2001JD000776
- 312 Cai, W., Ng, B., Wang, G. et al. Increased ENSO sea surface temperature variability under four IPCC
- emission scenarios. Nat. Clim. Chang. 12, 228–231 (2022). https://doi.org/10.1038/s41558-
- 314 022-01282-z
- Camargo, S.J., K.A. Emanuel and A.H. Sobel, 2007a. Use of a genesis potential index to diagnose
- 316 ENSO effects on tropical cyclone genesis. Journal of Climate, 20, 4819-4834, doi:
- 317 10.1175/JCLI4282.1.
- 318 Camargo, S.J., A.H. Sobel, A.G. Barnston, and K.A. Emanuel, 2007b. Tropical cyclone genesis
- potential index in climate models, Tellus, 59A, 428-443, doi:10.3402/tellusa.v59i4.15014.
- 320 Collins, M., An, SI., Cai, W. et al. The impact of global warming on the tropical Pacific Ocean and El
- 321 Niño. Nature Geosci 3, 391–397 (2010). https://doi.org/10.1038/ngeo868
- 322 Chu JE, Lee SS, Timmermann A et al (2020) Reduced tropical cyclone densities and ocean effects due
- 323 to anthropogenic greenhouse warming. Sci Adv 6(51):eabd5109
- 324 Coats, S., and K. B. Karnauskas, 2017: Are simulated and observed 20th century tropical Pacific sea
- 325 surface temperature trends significant relative to internal variability? Geophys. Res. Lett., 44,
- 326 9928–9937, doi: 10.1002/2017GL074622.

327 Coats, S., and K. B. Karnauskas, 2018: A role for the Equatorial Undercurrent in the ocean dynamical thermostat. J. Climate, 31, 6245–6261, doi: 10.1175/JCLI-D-17-0513.1. 328 329 Danabasoglu, G., Lamarque, J.-F., Bacmeister, J., Bailey, D. A., DuVivier, A. K., Edwards, J., et al. 330 (2020). The Community Earth System Model Version 2 (CESM2). Journal of Advances in Modeling Earth Systems, 12, e2019MS001916. https://doi.org/10.1029/2019MS001916 331 332 Drouard, M., and C. Cassou, 2019: A Modeling- and Process-Oriented Study to Investigate the 333 Projected Change of ENSO-Forced Wintertime Teleconnectivity in a Warmer World. J. Climate, 32, 8047–8068, https://doi.org/10.1175/JCLI-D-18-0803.1. 334 335 Emanuel, K. (2005). Increasing destructiveness of tropical cyclones over the past 30 years. Nature, 336 436(7051), 686–688. https://doi.org/10.1038/nature03906 337 Emanuel, K., R. Sundararajan, and J. Williams, 2008: Hurricanes and global warming: Results from downscaling IPCC AR4 simulations. Bull. Amer. Meteor. Soc., 89, 347–367, 338 doi:10.1175/BAMS-89-3-347. 339 Emanuel, K. A. and Nolan, D. S. 2004. Tropical cyclone activity and global climate. In: Proc. of 26th 340 Conference on Hurricanes and Trop- ical Meteorology, pp. 240–241, American 341 342 Meteorological Society, Miami, FL. Fredriksen, H.-B., Berner, J., Subramanian, A. C., & Capotondi, A. (2020). How does El Niño-343 344 Southern Oscillation change under global warming—A first look at CMIP6. Geophysical 345 Research Letters, 47, e2020GL090640. https://doi.org/ 10.1029/2020GL090640 Goldenberg, S. B., and L. J. Shapiro (1996), Physical mechanisms for the association of El Niño and 346 347 West African rainfall with Atlantic major hurricane activity, J. Clim., 9, 1169–1187. Gray, W. M., 1968: Global view of the origin of tropical disturbances and storms. Mon. Wea. Rev., 348 349 96, 669-700.

- 350 Gray, W. M. (1990), Strong association between West African rainfall and US landfall of intense 351 hurricanes, Science, 249(4974), 1251–1256. Heede, U. K., & Fedorov, A. V. (2021). Eastern equatorial Pacific warming delayed by aerosols and 352 353 thermostat response to CO2 increase. Nature Climate Change, 11(8), 696-703. Heede, U. K., & Fedorov, A. V. (2023a). Colder eastern equatorial Pacific and stronger Walker 354 355 circulation in the early 21st century: separating the forced response to global warming from 356 natural variability. Geophysical Research Letters, 50(3), e2022GL101020. 357 Heede, U.K., Fedorov, A.V. Towards understanding the robust strengthening of ENSO and more 358 frequent extreme El Niño events in CMIP6 global warming simulations. Clim Dyn (2023b). https://doi.org/10.1007/s00382-023-06856-x 359 360 Hersbach, H, Bell, B, Berrisford, P, et al. The ERA5 global reanalysis. Q J R Meteorol Soc. 2020; 146: 1999–2049. https://doi.org/10.1002/qj.3803 361 Huang, B., and Coauthors, 2017: Extended Reconstructed Sea Surface Temperature, Version 5 362 (ERSSTv5): Upgrades, Validations, and Intercomparisons. J. Climate, 30, 8179–8205, 363 https://doi.org/10.1175/JCLI-D-16-0836.1. 364 365 Hurrell, J. W., J. J. Hack, D. Shea, J. M. Caron, and J. Rosinski, 2008: A New Sea Surface Temperature
- Karnauskas, K. B., R. Seager, A. Kaplan, Y. Kushnir, and M. A. Cane, 2009: Observed strengthening
   of the zonal sea surface temperature gradient across the equatorial Pacific Ocean. J. Climate,
   22(16), 4316–4321, doi: 10.1175/2009JCLI2936.1.

and Sea Ice Boundary Dataset for the Community Atmosphere Model. J. Climate, 21, 5145-

366

367

5153,

Karnauskas, K. B., J. Jakoboski, T. M. S. Johnston, W. B. Owens, D. L. Rudnick, and R. E. Todd, 2020: The Pacific Equatorial Undercurrent in Three Generations of Global Climate Models

- and Glider Observations. J. Geophys. Res.-Oceans, 125(11), e2020JC016609, doi:
- 374 10.1029/2020JC016609.
- 375 Karnauskas, K. B., L. Zhang, and K. Emanuel, 2021: The feedback of cold wakes on tropical cyclones.
- 376 Geophys. Res. Lett., 48(7), e2020GL091676, doi: 10.1029/2020GL091676.
- 377 Klotzbach, P., S. Bowen, R. Pielke, and M. Bell, 2018: Continental United States hurricane landfall
- frequency and associated damage: Observations and future risks. Bull. Amer. Meteor. Soc., 99,
- 379 1359–1376, https://doi.org/10.1175/BAMS -D-17-0184.1.
- Knapp, K. R., Kruk, M. C., Levinson, D. H., Diamond, H. J. & Neumann, C. J. The international best
- 381 track archive for climate stewardship (IBTrACS): unifying tropical cyclone best track data.
- 382 Bull. Am. Meteor. Soc. 91, 363–376 (2010).
- 383 Knutson, T. R., R. E. Tuleya, and Y. Kurihara, 1998: Simulated increase of hurricane intensities in a
- 384 CO2-warmed climate. Science, 279, 1018–1021, doi:10.1126/science.279.5353.1018.
- Knutson, T., S. J. Camargo, J. C. L. Chan, K. Emanuel, C-H Ho, J. Kossin, M. Mohapatra, M. Satoh,
- 386 M. Sugi, K. Walsh, and L. Wu, 2020: Tropical Cyclones and Climate Change Assessment: Part
- 387 II: Projected Response to Anthropogenic Warming. Bull. Amer. Meteor. Soc., 101, E303–
- 388 E322, https://doi.org/10.1175/BAMS-D-18-0194.1.
- 389 Knutson, T. R., and S. Manabe, 1995: Time-Mean Response over the Tropical Pacific to Increased
- 390 C02 in a Coupled Ocean-Atmosphere Model. J. Climate, 8, 2181–2199,
- 391 https://doi.org/10.1175/1520-0442(1995)008<2181:TMROTT>2.0.CO;2.
- 392 Lee, S., L'Heureux, M., Wittenberg, A.T. et al. On the future zonal contrasts of equatorial Pacific
- 393 climate: Perspectives from Observations, Simulations, and Theories. npj Clim Atmos Sci 5, 82
- 394 (2022). https://doi.org/10.1038/s41612-022-00301-2
- Lin, I-I, Camargo, SJ, Patricola, CM, Boucharel, J, Chand, S, Klotzbach, P, Chan, JCL, Wang, B,
- Chang, P, Li, T & Jin, F-F 2021, ENSO and Tropical Cyclones. in MJ McPhaden, A Santoso

397 & W Cai (eds), El Niño Southern Oscillation in a Changing Climate. Geophysical Monograph American Geophysical Union. 398 Series, vol. 253. 377-408. pp. 399 https://doi.org/10.1002/9781119548164.ch17 400 Maher, N., Wills, R. C. J., DiNezio, P., Klavans, J., Milinski, S., Sanchez, S. C., Stevenson, S., Stuecker, 401 M. F., and Wu, X.: The future of the El Niño-Southern Oscillation: using large ensembles to 402 illuminate time-varying responses and inter-model differences, Earth Syst. Dynam., 14, 413– 403 431, https://doi.org/10.5194/esd-14-413-2023, 2023. Murakami, H., and Coauthors, 2012: Future Changes in Tropical Cyclone Activity Projected by the 404 405 New High-Resolution MRI-AGCM. J. Climate, 25, 3237-3260, https://doi.org/10.1175/JCLI-D-11-00415.1. 406 407 National Oceanic and Atmospheric Administration. (2023), NOAA predicts a near-normal 2023 Atlantic hurricane season, Available from: https://www.noaa.gov/news-release/2023-408 atlantic-hurricane-season-outlook (Accessed 25 May 2023) 409 Peduzzi, P., B. Chatenoux, H. Dao, A. De Bono, C. Herold, J. Kossin, F. Mouton, and O. Nordbeck, 410 2012: Global trends in tropical cyclone risk. Nat. Climate Change, 2, 289-294, 411 412 https://doi.org/10.1038/nclimate1410. 413 Seager, R., N. Henderson, and M. Cane, 2022: Persistent Discrepancies between Observed and 414 Modeled Trends in the Tropical Pacific Ocean. J. Climate, 35, 4571-4584, https://doi.org/10.1175/JCLI-D-21-0648.1. 415 Seager, R., Cane, M., Henderson, N. et al. Strengthening tropical Pacific zonal sea surface temperature 416 417 gradient consistent with rising greenhouse gases. Nat. Clim. Chang. 9, 517-522 (2019). https://doi.org/10.1038/s41558-019-0505-x 418

- Sobel, A. H., C.-Y. Lee, S. G. Bowen, S. J. Camargo, M. A. Cane, A. Clement, B. Fosu, M. Hart, K. A.
- Reed, R. Seager, and M. K. Tippett (2023) Near-term tropical cyclone risk and coupled Earth
- 421 system model biases. In press at *Proc. Nat. Acad. Sci.*
- 422 Tang, B. H., and Neelin, J. D. (2004), ENSO Influence on Atlantic hurricanes via tropospheric
- 423 warming, Geophys. Res. Lett., 31, L24204, doi:10.1029/2004GL021072.
- 424 van Westen, R.M., Dijkstra, H.A. & Bloemendaal, N. Mechanisms of tropical cyclone response under
- climate change in the community earth system model. Clim Dyn (2023).
- 426 https://doi.org/10.1007/s00382-023-06680-3
- 427 Vecchi, G.-A., & Soden, B.-J. (2007). Global warming and the weakening of the tropical circulation.
- 428 Journal of Climate, 20(17), 4316–4340.
- 429 Villarini, G., and G. A. Vecchi, 2012: Twenty-first-century projections of North Atlantic tropical
- storms from CMIP5 models. Nat. Climate Change, 2, 604–607, doi:10.1038/nclimate1530.
- Wittenberg, A. T., 2009: Are historical records sufficient to con-strain ENSO simulations? Geophys.
- 432 Res. Lett., 36, L12702, doi:10.1029/2009GL038710.
- Zhang, L., K. B. Karnauskas, J. P. Donnelly, and K. Emanuel, 2017: Response of the North Pacific
- 434 Tropical Cyclone Climatology to Global Warming: Application of Dynamical Downscaling to
- 435 CMIP5 Models. J. Climate, 30(4), 1233–1243, doi: 10.1175/JCLI-D-16-0496.1.

# **Figures**

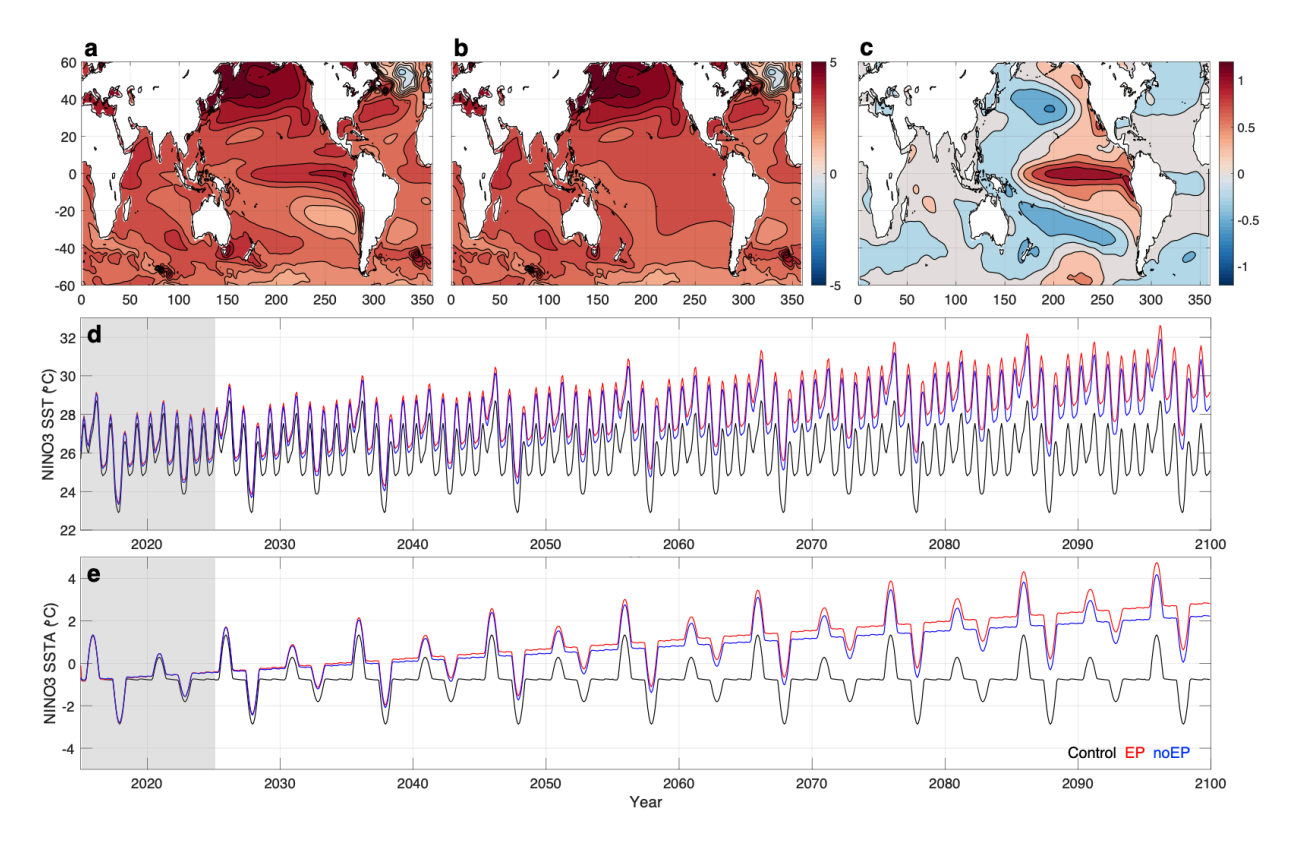
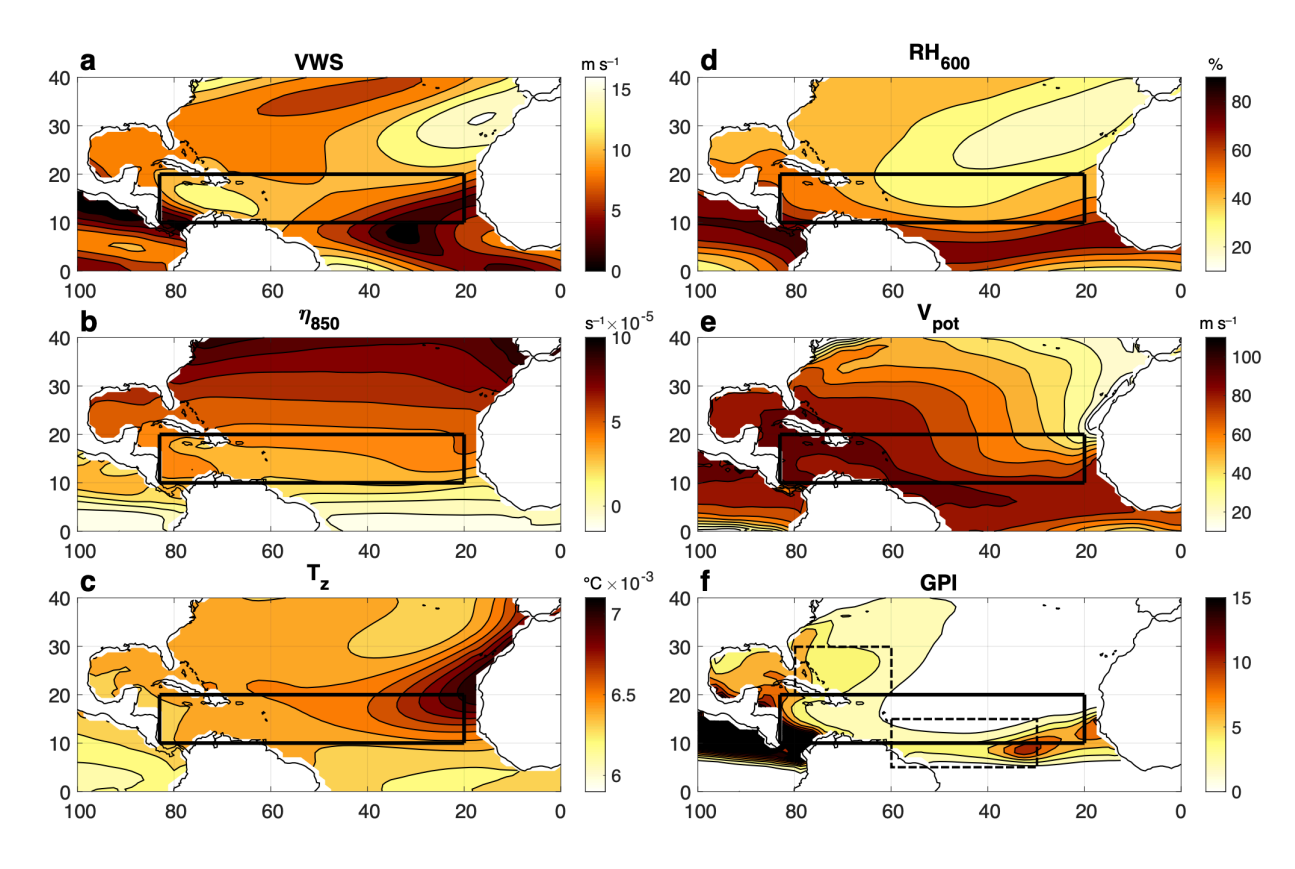
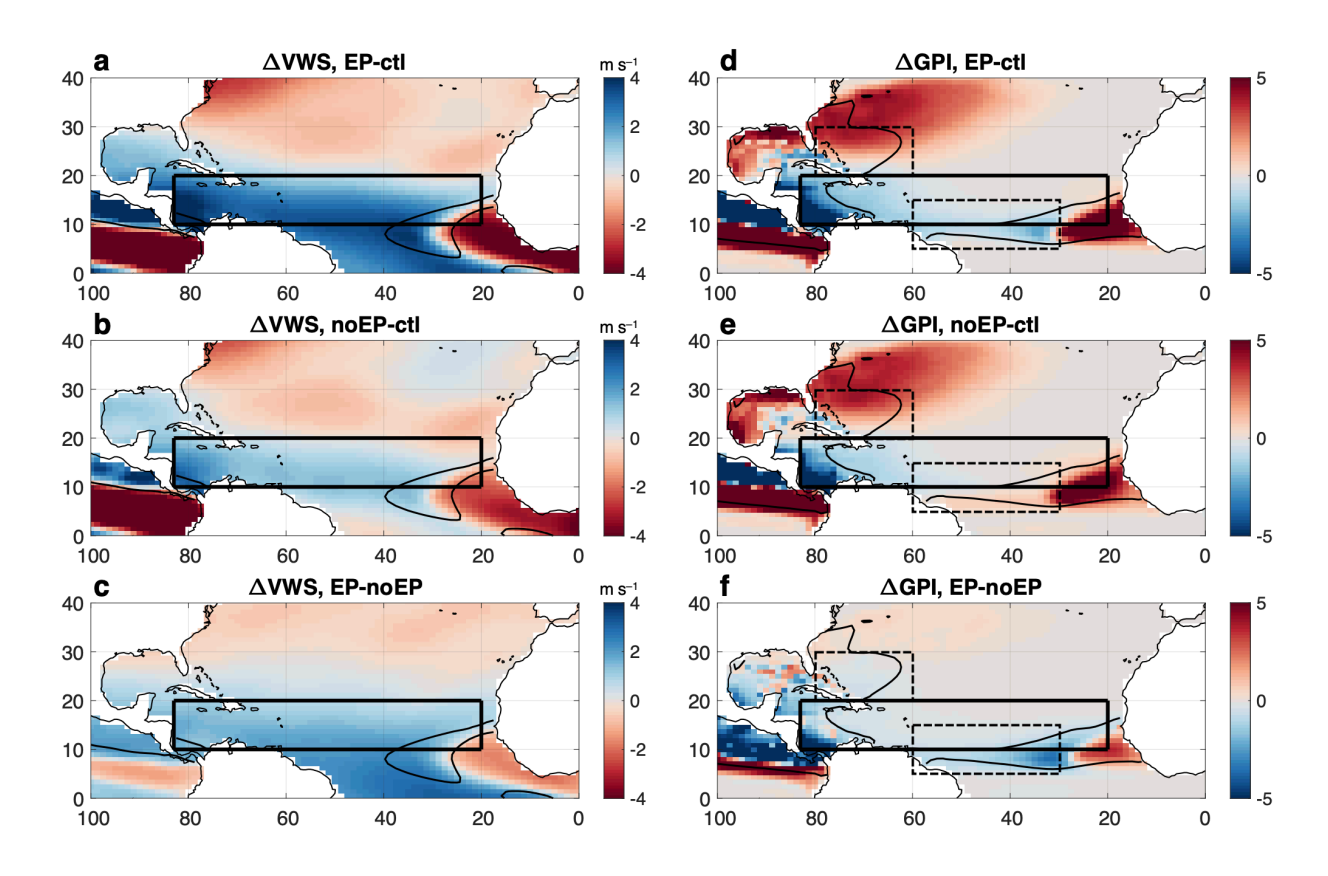


Figure 1. Spatial pattern of prescribed global warming pattern (a) including and (b) excluding enhanced eastern Pacific warming, composed as the SST difference (°C) between EP or noEP experiments averaged from 2090–2100 and the control experiment. (c) Spatial pattern of prescribed ENSO pattern, composed as SST anomalies (°C) in the control experiment regressed onto the NINO3 index in the control experiment. (d) Time series of SST in the NINO3 region in the control (black), EP (red) and noEP (blue) experiments. (e) As in d but with the seasonal cycle removed, and the time series aligned by subtracting the average of the first year of each time series. The gray shaded region in d and e marks the first 10-year segment; the prescribed ENSO sequence repeats every 10 years, as described in Section 2.



**Figure 2.** (a) Vertical wind shear between 250 mb and 850 mb (m s<sup>-1</sup>), (b) 850-mb absolute vorticity (s<sup>-1</sup>), (c) vertical temperature gradient between 850 mb and 250 mb (°C m<sup>-1</sup>), (d) 600-mb relative humidity (%), (e) potential intensity (m s<sup>-1</sup>), and (f) genesis potential index during hurricane season (June–November) averaged over the control experiment. Color scales are oriented such that darker implies greater genesis potential. The thick black rectangle denotes the main development region. The dashed rectangles in f denote the regions used for bar charts in Figure 5. Equivalent fields calculated from ERA5 over the period 1991–2020 are provided in Figure S1.



**Figure 3.** (a) Change in vertical wind shear (m s<sup>-1</sup>) during hurricane season (June–November) at 2080–2100 in the EP experiment relative to the control experiment. For reference, the 4 m s<sup>-1</sup> wind shear contour from Figure 2a (control) and the MDR are plotted. (b) As in a but for the noEP experiment. (c) Difference between wind shear during hurricane season at 2080–2100 in the EP experiment relative to the noEP experiment. (d)–(f) As in a–c, but for genesis potential index, and the GPI = 4 contour from Figure 2f (control) is plotted for reference. The dashed rectangles in d–f denote the regions used for bar charts in Figure 5.

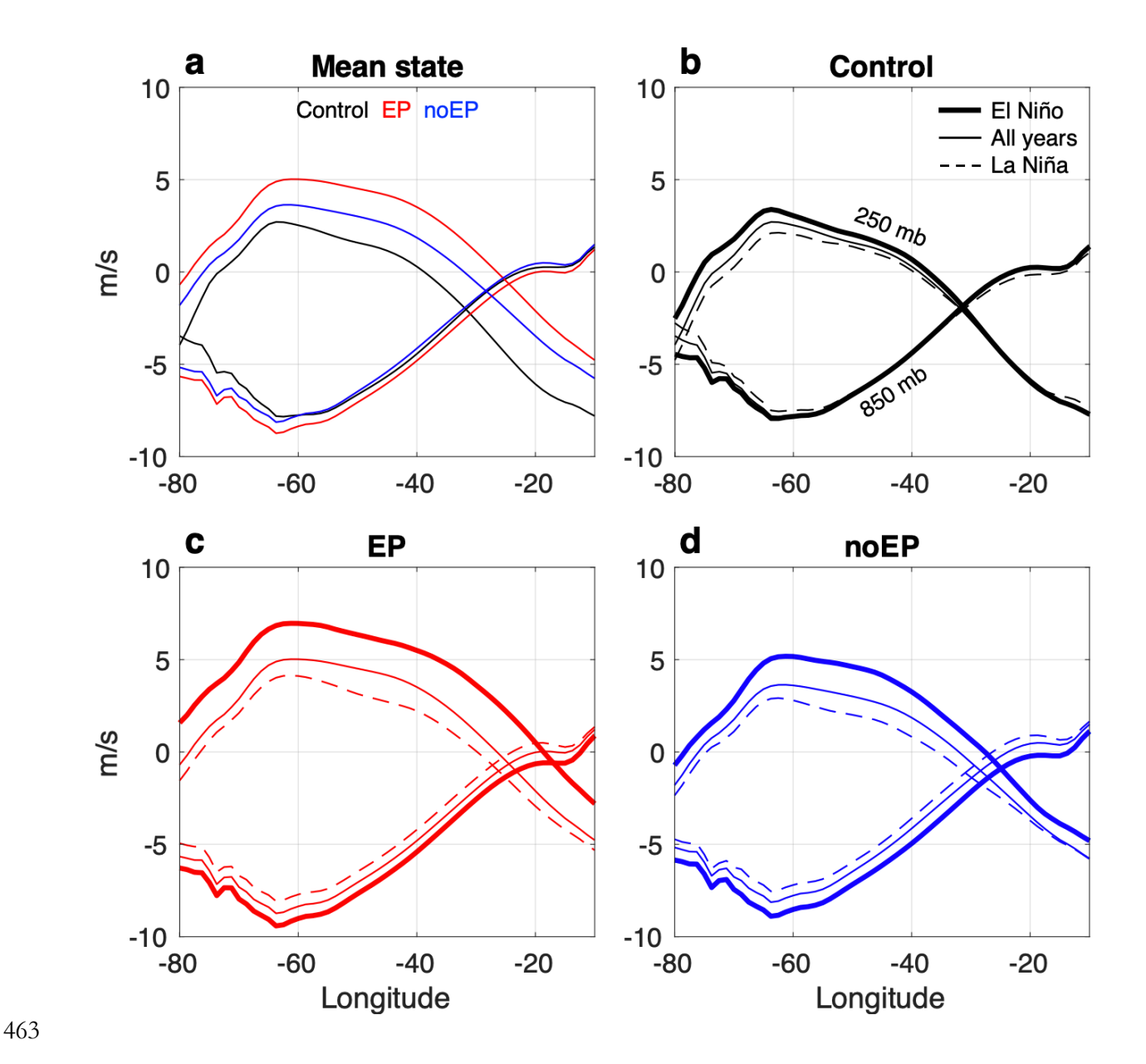


**Figure 4.** (a) Profiles of zonal wind at 850 mb and 250 mb averaged from 8–11°N during hurricane season in the control experiment (black), EP experiment at 2080–2100 (red), and noEP experiment at 2080–2100 (blue). (b) ENSO signal in zonal wind profiles in the control experiment: El Niño (thick), all years (thin solid), and La Niña (thin dashed). (c) As in b, but for the EP experiment at 2080–2100. (d) as in b, but for the noEP experiment at 2080–2100. Within this latitudinal range, the coast of Africa is at approximately 14°W.

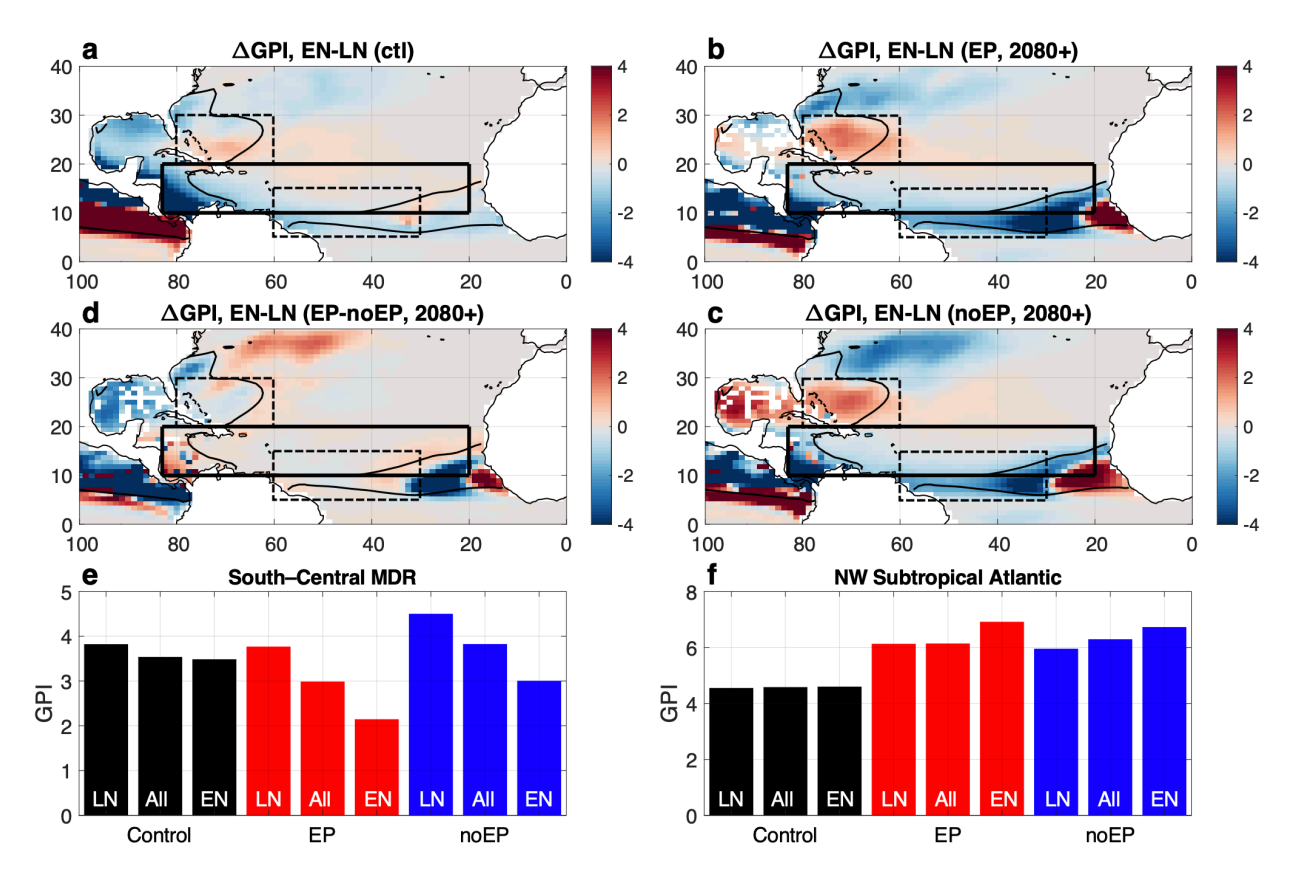


Figure 5. (a) ENSO signal in hurricane season GPI in the control experiment, composed as the difference between GPI during strong El Niño and strong La Niña events. For reference, the GPI = 4 contour and the MDR are plotted. (b) As in a, but taken over 2080–2100 in the EP experiment. (c) As in b, but for the noEP experiment. (d) Difference in the ENSO signal in hurricane season GPI at 2080–2100 between the EP and noEP experiments. The dashed rectangles in a–d denote the regions used for bar charts in e–f. Outliers in the Gulf of Mexico in b–d arising due to noise in the CAPE field (part of the potential intensity calculation and thus part of GPI) are masked white. (e) Hurricane season GPI in the control experiment (black bars), EP experiment (red bars), and noEP experiment (blue bars) averaged over La Niña years (LN), all years (All), and El Niño years (EN), averaged over the south-central MDR (60–30°W x 5–15°N). (f) As in e but for the northwestern subtropical Atlantic (80–60°W x 20–30°N).